Fast Speed Control of AC Machines Without the Proportional-Integral Controller: Using an Extended High-Gain State Observer

Fengxiang Wang, *Senior Member, IEEE*, Junxiao Wang, *Member, IEEE*, Ralph M. Kennel, *Senior Member, IEEE*, and José Rodríguez, *Fellow, IEEE*

***Abstract*—As cascaded proportional-integral controllers involve complicated tuning work, many efforts have been focused on direct controllers. Direct torque control and predictive torque control are both feasible solutions. However, bigger ripples or weighting factor designs are not easily solved. In this paper, a direct current controller that uses an extended high-gain state observer is proposed. The integral controller is removed from the system by using a disturbance estimation technique, which improves the system's performance with a variety of loads. A direct current controller without weighting factors is proposed as the inner controller. Unlike existing direct control methods, all phase currents are considered equally in the controller, which ensures a high current control quality. The simulation and experimental results verify that the proposed method performs well both in steady and transient states.**

***Index Terms*—AC machines, fast speed control, state observer.**

I. Introduction

ELECTRICAL machine systems are the key components of almost all intelligent equipment. Different machine topologies have been developed for various applications. Generally, induction machines and PMSMs are the most-used machines [1]–[7]. The field-oriented control (FOC) method decouples the flux and torque control, and has become the most widely used motor control method. However, the cascaded proportional-integral (PI) structure has many parameters

Manuscript received May 24, 2018; revised July 17, 2018 and September 30, 2018; accepted December 20, 2018. Date of publication December 27, 2018; date of current version June 10, 2019. This work was supported in part by the National Natural Science Foundation of China under Grants 51877207, 61803335, and U1709213, in part by the CONICYT-Basal Project FB0008, and in part by the Fondecyt Project 1170167. Recommended for publication by Associate Editor B. Fahimi. *(Corresponding author: Junxiao Wang.)*

F. Wang is with Quanzhou Institute of Equipment Manufacturing, Haixi Institutes, Chinese Academy of Sciences, Jinjiang 362201, China (e-mail:

predicted currents and their references. The basic principle of the direct current controller is that every phase current is controlled with the same importance. Unlike PTC method, the proposed current control method considers phase currents as the controlled variables in the cost function, With this design, there are no weighting factors in the cost function. In classical predictive current control (PCC), the cost function handles stator current errors in the α and β axes as the main consideration, the PCC system has no weighting factor. In our experience, classic PCC works. However, it has not been optimized so as to truly control each phase current equally. In other words, an equal control of the α and β axes does not lead to an equal control of each phase of *a*, *b*, and *c*. The proposed method guarantees the high quality of currents in all axes, which is essential for the control of drives systems, especially low-power drives.

Furthermore, a disturbance estimation based technique is researched for substituting the outer PI loop [29]–[36]. In process controls, the disturbance estimation based method has been widely researched and investigated. It has been proved that it is a very good strategy for solving the problems of load disturbance and uncertainties [19], [23]–[28]. The considered disturbance observer means that the integral part is no longer required. In this paper, by considering the features of induction machines, an extended high-gain state observer based direct current control method is presented. The proposed system uses a load disturbance based technique as the outer speed controller and applies a direct current controller as the inner loop. The proposed control structure eliminates integration from the motor control system. Fast dynamics are guaranteed. Moreover, there is no weighting factor for the inner controller. Very good current qualities are obtained easily in various applied ranges. The experimental results are presented to verify the effectiveness of the proposed strategy.

This paper is structured as follows. Section II presents the mathematical model of the induction machine. Section III gives the design of the proposed control method. Section IV provides the experimental results. Section V presents the conclusion of this paper. Some calculations for the current controller are presented in the Appendix.

II. Hardware System Model

A squirrel-cage induction machine (IM) serves as the test motor for this paper. It is described by a set of classic electrical and mechanical equations in stationary reference frame as follows:

$$\upsilon_s = R_s \cdot i_s + \frac{d}{dt}\psi_s \tag{1}$$

$$0 = R_r \cdot i_r + \frac{d}{dt}\psi_r - j \cdot \omega_e \cdot \psi_r \tag{2}$$

$$\psi_s = L_s \cdot i_s + L_m \cdot i_r \tag{3}$$

$$\psi_r = L_r \cdot i_r + L_m \cdot i_s \tag{4}$$

$$\frac{d\omega}{dt} = \frac{T_e}{J} - \frac{T_L}{J} - \frac{B\omega}{J} \tag{5}$$

$$T_e = \frac{3}{2} \cdot p \cdot Im(\psi_s^* \cdot i_s). \tag{6}$$

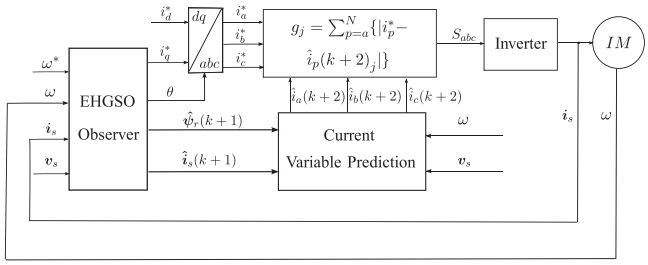

Fig. 1. Block diagram of disturbance observer based PCC scheme.

In the above equations, υ_s is the stator voltage vector; and ψ_s and ψ_r represent the stator flux and rotor flux, respectively. i_s and i_r are the stator and rotor currents, respectively. R_s and R_r are the stator and rotor resistances, respectively. L_s, L_r, and L_m are stator, rotor, and mutual inductances, respectively; ω, and ω_e are the mechanical and electrical speeds, respectively. p is the number of pole pairs, T_L is load torque, B is viscous friction coefficient, J is the moment of inertia, and T_e denotes the electromagnetic torque.

III. Integration Elimination Based Direct Current Control

In this paper, we focus on high performance control system design. The control system includes two main parts: the inner controller and the external controller. Traditionally, both controllers use the PI method. However, this method has the disadvantage of requiring extensive parameter tuning work due to its cascaded PI structure. It also presents the problem of slow dynamics because the inner bandwidth limits the external one. In our system, as shown in Fig. 1, a direct current control using a cost function without any weighting factors is proposed as the inner controller, and a disturbance observer based scheme is designed as the external speed controller. With this design of control system design, we try to achieve high quality performance of current and torque in both steady and transient states. The theory design and test results will verify the proposed system.

A. Inner Controller: Direct Current Control Without Weighting Factors

The inner controller directly generates the control signals for the inverter. FOC uses continuous voltage references to carry out a pulsewidth modulation that will control the status of the switches. The current controller in a FOC system refers to at least four parameters for inner PI controllers. DTC applies direct switching signals through a pre-defined LUT. With the exception of the LUT design, the DTC method has at least two parameters for torque and flux hysteresis controllers. PTC takes all feasible switching vectors into consideration in the controller design. The one that minimizes the cost function will be selected as the output. The PTC method has at least one weighting factor to be tuned in the cost function, which is used to weight the importance of torque and stator flux magnitude. However, according to our experience, it is impossible to

maintain the system's stability at different operation points when using constant values for weighting factors.

From another view of control, a multi-phase machine has multi-phase currents. If we could achieve more exact control of every phase current, especially for low power machines, the machine could be expected to perform very well. By considering this idea and one step prediction, a cost function that consists of N phase currents is designed by considering all phase current errors equally as follows:

$$g_j = \sum_{p=a}^{N} \{|i_p^* - \hat{i}_p(k+1)_j|\} \tag{7}$$

where p denotes phase and is equal to a, b, c, ... The symbol j expresses the number of vectors. For the applied two-level, three-phase inverter, there are eight possible switching signals, but only produces seven different voltage vectors. Thus, for this proposed method, $j = 0, \ldots, 6$, which means that the cost function must be considered and calculated seven times within every control period in order to select the optimal switching control signal. The three phase currents are considered equally important. Therefore, there are no weighting factors in the cost function.

From (7), it can be seen that the cost function is very interesting and practical. The controller is very simple to understand. This idea could be used in almost all motor systems. For three-phase motors, N is equal to a, b, and c. The most important point is that there are no parameters to be tuned. Every phase current is controlled equally, and this is done with accuracy at each of the different operation points. In this paper, we use a three-phase induction machine as the test object. In the implementation, we need to consider the time-delay problem and system constraints. To simplify the system design, we only consider over-current protection for system safety. The cost function is designed as follows:

$$\begin{aligned} g_j = \sum_{h=1}^{N} \{&|i_a^* - \hat{i}_a(k+h)_j| + |i_b^* - \hat{i}_b(k+h)_j| \\ &+ |i_c^* - \hat{i}_c(k+h)_j| + I_m(k+h)_j\} \end{aligned} \tag{8}$$

where h is the prediction horizon. $I_m(k+h)$ is the term to constrain the currents. It generates an unlimited value when the tested switching states generate an over-current prediction value. Therefore, the switching vectors that cause system over-current will never be selected as the output. In a real system, considering the time-delay problem, we set h equal to 2 to compensate for one-step predictive control. Long step predictions could further improve the system performance. However, there must be more efforts to overcome the model's parameter problem that is caused by multi-step errors. This falls outside the scope of this paper and is left for a future work. The calculations of the predictive variables like $i(k+1)$, the time-delay compensation $i(k+1)$ and the reference $i_{a,b,c}^*$ are presented in the Appendix of this paper.

B. External Speed Controller: Extended High-Gain State Observer Based Speed Control System

As we know, the cascaded control structure for IM systems is widely used in most industrial applications. The PI controller is designed in the speed loop; it is described as

$$\begin{aligned} \dot{e}_\omega &= \dot{\omega}_r - \dot{\omega} = -k_t i_q^* + d_\omega(t), k_t = \frac{3pL_{m0}\psi_r}{2L_{r0}J_0} \\ d_\omega(t) &= -\frac{3pL_{m0}\psi_r}{2L_{r0}J_0} i_q^* + \frac{3pL_m\psi_r}{2L_rJ} i_q - \frac{T_L}{J} - \frac{B\omega}{J} \\ k_t i_q^* &= -k_p \cdot e_\omega - k_i \cdot \int e_\omega . \end{aligned} \tag{9}$$

From (9), it is easy to see that the disturbances are canceled by an integral term. Notice that the lumped disturbances are caused by torque, friction, and so on. The integral effect has two disadvantages. First, it cannot deal with many complex conditions. For example, the resistance and inductance parameter values are time-varied with operation temperature and current; they are not constant values. Second, this feedback regulation is slow. The speed drop or ripples injected by disturbances are settled by an integration process, which is slow. The feed-forward compensation scheme could be introduced as a good solution that can estimate the disturbance within one sampling interval.

For observing the lumped disturbances caused by torque load changes and parameter variation, based on the speed mathematical model (5), the speed equation can be rewritten as $\dot{\omega} = k_t i_q^* + d_\omega(t), k_t = \frac{3pL_{m0}\psi_r}{2L_{r0}J_0}$ where i_q^* is the q-axis current reference, and the lumped disturbance is denoted as $d_\omega(t) = -\frac{3pL_{m0}\psi_r}{2L_{r0}J_0} i_q^* + \frac{3pL_m\psi_r}{2L_rJ} i_q - \frac{T_L}{J} - \frac{B\omega}{J}$. On the basis of the disturbance estimation technique, the disturbance estimation $\hat{d}_\omega(t)$ is designed as

$$\begin{cases} \dot{z}_1 = k_t i_q^* + z_2 + (\alpha_1/\xi)(\omega - z_1) \\ \dot{z}_2 = (\alpha_2/\xi^2)(\omega - z_1) \end{cases} \tag{10}$$

where $z_1 = \hat{\omega}, z_2 = \hat{d}_\omega(t)$, and $\alpha_1, \alpha_2, \xi > 0$.

Assumption 3.1: For the induction motor system, suppose that lumped disturbances $d(t)$ are constants or bounded in steady state, i.e., $\lim_{t\to 0} \dot{d}(t) = 0$ or $\leq l$.

Lemma 3.1 (see [38]): Consider a nonlinear system $\dot{x} = F(x, w)$, where $x(t)$ and $w(t)$ are the system state and control input, respectively, and are input-to-state stable (ISS). If the input satisfies $\lim_{t\to 0} w(t) = 0$, then the system states satisfy $\lim_{t\to 0} x(t) = 0$.

For the system of (10), define

$$\begin{cases} e_\omega(t) = (\omega - z_1)/\xi \\ e_d(t) = d_\omega(t) - \hat{d}_\omega(t). \end{cases} \tag{11}$$

Taking the time derivative of $e_\omega(t), e_d(t)$ yields

$$\begin{cases} \xi \dot{e}_\omega(t) = e_d - \alpha_1 e_\omega \\ \xi \dot{e}_d(t) = \xi \dot{d}_\omega - \alpha_2 e_\omega . \end{cases} \tag{12}$$

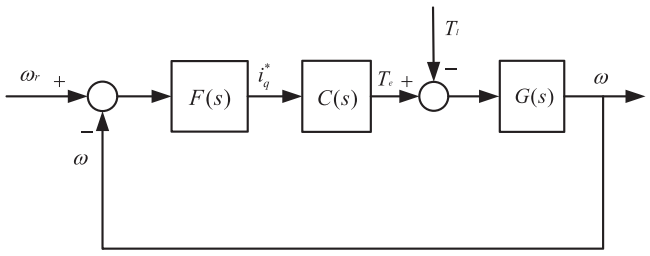

Fig. 2. Simplified diagram for IM control system in frequency domain.

The Lyapunov function is defined as follows:

$$V_{e_d} = \frac{\xi}{2}e_d^2 + \frac{\alpha_2 \xi}{2}e_\omega^2 \tag{13}$$

where $\xi, \alpha_2 > 0$.

Taking the time derivative of V_{e_d}, using (12) yields

$$\begin{aligned}\dot{V}_{e_d} &= e_d(\xi \dot{d}_\omega - \alpha_2 e_\omega) + \alpha_2 e_\omega (e_d - \alpha_1 e_\omega) \\ &= -\alpha_1 \alpha_2 e_\omega^2 + \xi e_{d_1} \dot{d}_\omega . \end{aligned} \tag{14}$$

If the induction motor system satisfies Assumption 3.1, then the error system (12) is ISS. Noting that $\lim_{t\to 0} \dot{d}_\omega(t) = 0$, according to Lemma 3.1, then it can be concluded that $\lim_{t\to 0} e_d(t) = 0, \lim_{t\to 0} e_\omega(t) = 0$, where $\alpha_1, \alpha_2 > 0$, and the error states of (12), will converge to the desired equilibrium point asymptotically.

Fig. 2 shows the simplified diagram for control system in frequency domain, $F(s)$ denotes the speed controller, $C(s) = \frac{1}{T_c S+1}$ is the transfer function of current loop, $G(s) = \frac{1}{JS}$ describes the control object. Then, based on these function, the frequency analysis is proceed, the transfer function of PI control based open-loop system could be derived as

$$G_p(s) = \frac{k_i + k_p S}{JT_c S^3 + JS^2}. \tag{15}$$

The proposed controller based open-loop system transfer function could be derived as (16) shown at the bottom of this page.

From Fig. 3, it could be seen that fast transient response is achieved with larger parameter value using PI method. However, the phase margin become small and results in an overshoot, even cause the system instability. There is a tradeoff for system rapidity and stability. The proposed control scheme is investigated and it may improve the system performance for better results shown in Fig. 4.

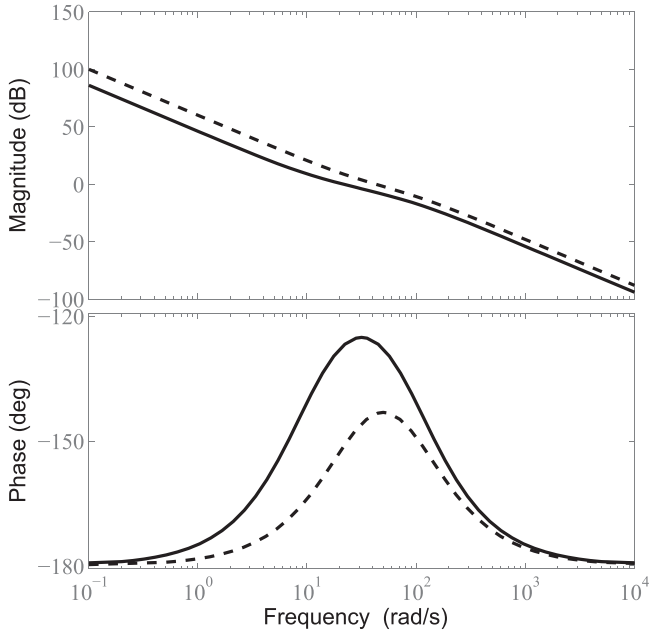

Fig. 3. Bode plots of PI method based control system.

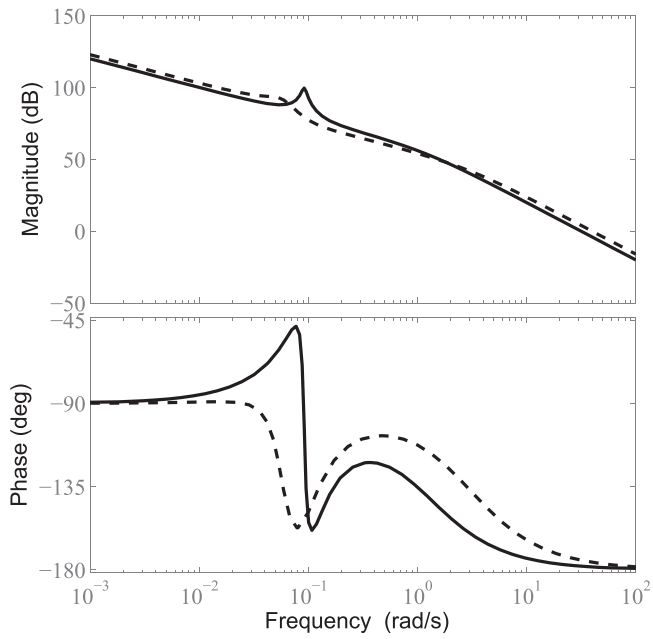

Fig. 4. Bode plots of the proposed algorithm based control system.

IV. Simulation and Experimental Results

A. Simulation Results

The main induction motor parameters used in these tests are given in Table I. The main motor has rated power of 2.2 kW with one pole pair. It has rated torque of 7.5 Nm with a nominal current of 4.61 A. More details are listed in Table I. They are obtained from the motor tested in the laboratory. The sampling frequency is 16 kHz. The parameters selected for the extended high gain state observer-direct current control (EHGSO-DCC) controller are $k_p = 0.06, \alpha_1 = 10, \alpha_2 = 100$.

To investigate performance of the proposed algorithm, the simulation work includes both transient and steady states. Comparison of the proposed current control and the classical one is discussed in this part to show the advantages of the

$$G_d(s) = \frac{k_p k_t \xi^2/\alpha_2 S^2 + k_p k_t \xi \alpha_1/\alpha_2 S + k_p k_t}{\xi^2 JT_c/\alpha_2 S^4 + (\xi^2 J/\alpha_2 + \xi\alpha_1 JT_c/\alpha_2)S^3 + (\xi\alpha_1 J/\alpha_2 + (1-k_t)JT_c/\alpha_2)S^2 + ((1-k_t)J + k_t^2)S} \tag{16}$$

TABLE I
PARAMETER VALUES OF INDUCTION MOTOR

Descriptions	Parameters	Nominal Values
DC link Voltage	V_{dc}	582 (V)
Stator Resistance	R_s	2.68 Ω
Rotor Resistance	R_r	2.13 Ω
Mutual Inductance	L_m	275.1 (mH)
Stator Inductance	L_s	283.4 (mH)
Rotor Inductance	L_r	283.4 (mH)
Pole Pairs	P	1.0
Speed	ω_{nom}	2772.0 (RPM)
Stator Flux	$\lvert\psi_s\rvert_{nom}$	0.99 Wb
Current	i_{nom}	4.61 A
Torque	T_{nom}	7.5 (Nm)
Inertia	J_{nom}	0.005 $kg \cdot m^2$

proposed system. In [9] and [18], a cost function of classical PCC is presented as following:

$$g_j = \sum_{h=1}^{N} \{|i_\alpha^* - \hat{i}_\alpha(k+h)_j| + |i_\beta^* - \hat{i}_\beta(k+h)_j| + I_m(k+h)_j\}. \quad (17)$$

In this cost function, currents are calculated in i_α, i_β frame. It has no weighting factor, but it does have a coefficient. We often ignore this point by traditionally using a weighting factor of one. The cost function in (17) cannot express exactly the equal control of each phase current as the proposed method in this paper did. At some operation points, in (17), a coefficient unequal to one could get better results than the value of one (no weighting factor). Plenty of tests have verified this point during our work. It means that the classical method with (17) has a problem of adaptable weighting factor design. However, the use of proposed (8) guarantees good performance at all operation points without weighting factors. In. Figs. 5 and 6, classical PCC with coefficient of one and the proposed method are compared. From the general view of rotating from zero to high speed with a full load disturbance, speed, torque, and current are depicted. As a response of full external torque loaded, driving current increased synchronously. Direct current methods guarantee a fast and stable performance during this dynamic process. From pictures, it may conclude that both methods achieves accepted results with stable speed, low torque ripples and high current qualities. For direct control methods like DTC, operation point of low speed with big load is challenging. To verify the effectiveness of the proposed system, behavior at 300 rpm with full load is investigated. The performance of speed, torque, and phase current under (17) and the proposed (8) are depicted in Figs. 7 and 8, respectively. The torque ripples in Fig. 7 with classical method are around 2.2 Nm, which is bigger than a value of 1.9 Nm in Fig. 8 with the proposed algorithm. With

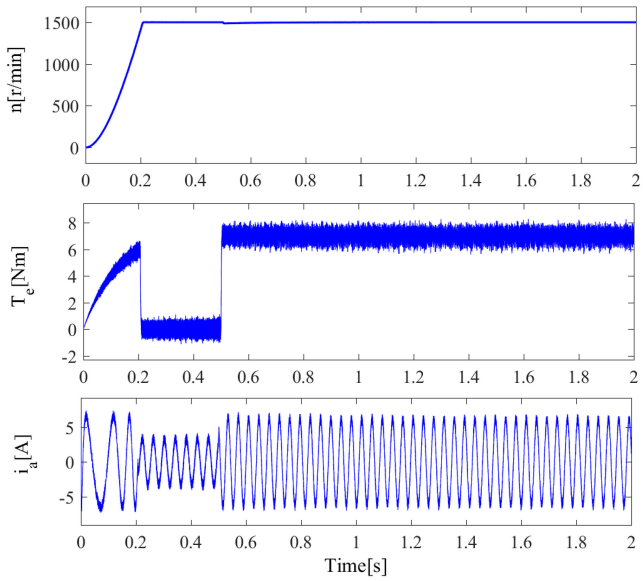

Fig. 5. Speed, torque, and i_a waveforms at full load when in high speed operation under classic method.

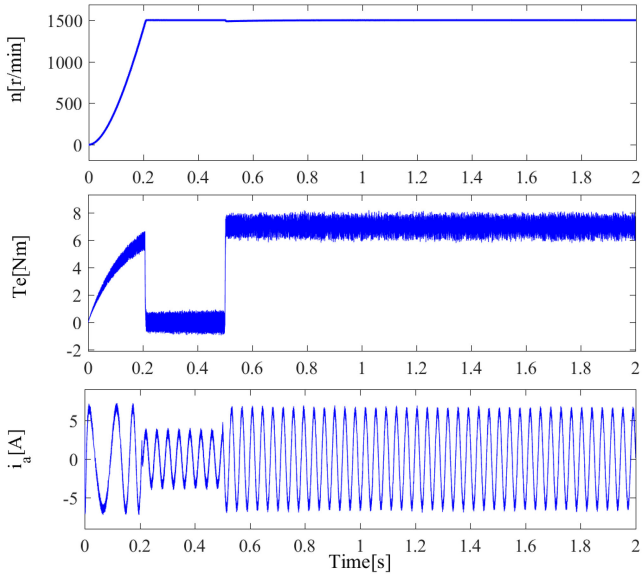

Fig. 6. Speed, torque, and i_a waveforms at full load when in high speed operation under proposed method.

a calculation of current total harmonic distortion (THD), the proposed method has result of 3.9%, which is slightly better than 4.5% in the classical scheme. The reason could be analyzed in theories. Though both methods using the same current predictions, different cost function decides the final results. In (17), errors in α and β are evaluated. However, a coefficient lacks of standard or optimized formers. A fixed weighting factor cannot work with the best results at different operation points. An adaptable value is not easy to be defined. In (8), the cost function considers three phase currents. Without weighting factors, each phase current is considered with the same importance equally, which is expected in machine systems. The following sections present experimental results of the proposed method for proving the effectiveness.

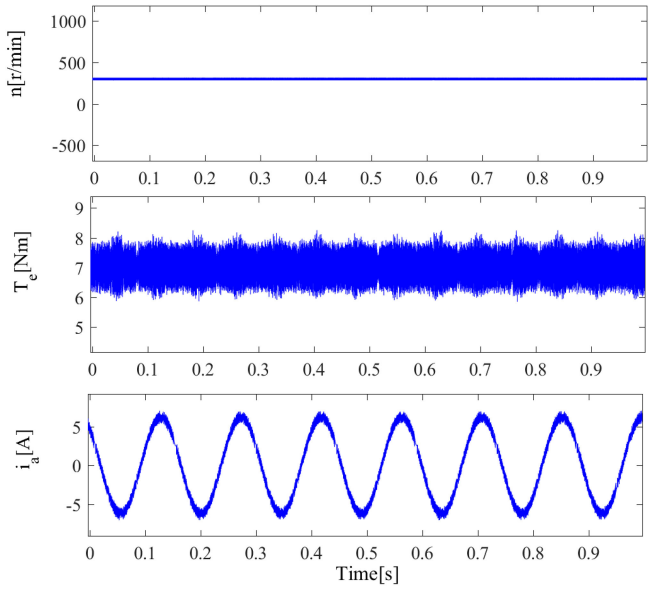

Fig. 7. Speed, torque, and i_a waveforms at full load under classic method.

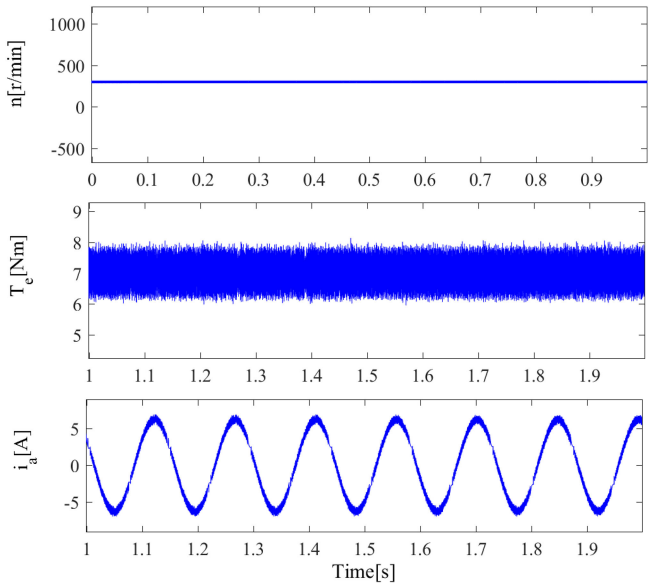

Fig. 8. Speed, torque, and i_a waveforms at full load under proposed method.

B. Experimental Results

The proposed EHGSO-DCC method has been verified on an experimental setup, as shown in Fig. 9. The platform includes two induction motors. The tested motor is driven and controlled by a Servostar 620 inverter, which opens the gates of the IGBTs for the real-time Pentium computer system. The load machine is driven by a Danfoss inverter. The current feedback information is obtained via the A/D data card from current sensors measurement. This system adopts a 1024-point incremental encoder for obtaining position information. Table I provides the parameters of the induction motor. It uses C program for the controller implementation. The implementation of the whole program is less than 50 μs, which is less than the sampling interval 60 μs.

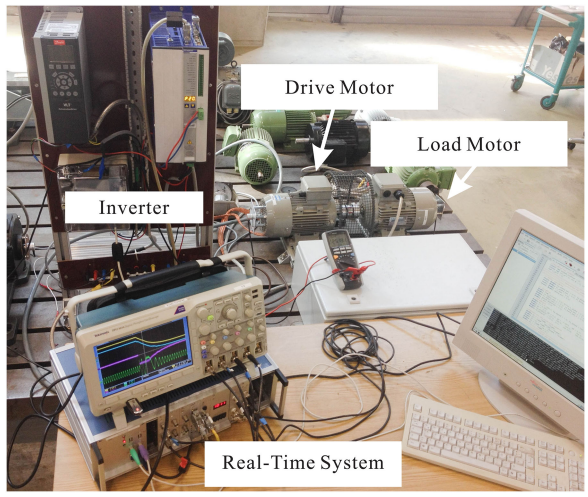

Fig. 9. Experimental setup description.

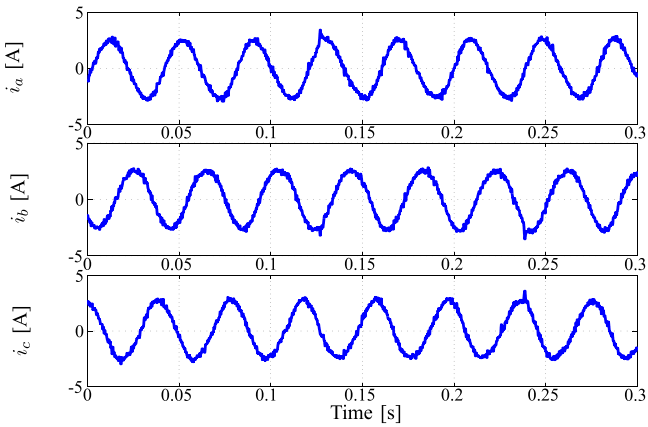

Fig. 10. Current waveforms of a, b, c phases under classic method (THD = 8.79%).

The first set of test is for performance comparison between the classic method and proposed method. As we know, motor has worse current results under condition of zero load, to investigate the behaviors of currents, an operation point of full speed without load is selected. To take a close look at the three phase currents in steady state, experimental results of classical method and the proposed one as depicted in Figs. 10 and 11, respectively. It can be seen that the three phase currents of the proposed current controller have equal and the same qualities, which could also be concluded from the cost functions design. The THD resulted of the proposed method is 5.87%, which is better than the classic method of 8.79%. In addition, in real operations, the motor always works with loads. The performance at full speed with a sudden full load disturbance is verified. This test is very interesting, because it considers the nominal values of speed and load; we observe not only steady behaviors but also a dynamic process in this operation. Figs. 12 and 13 show the results for the classical method and the proposed one, respectively. It could be seen that the proposed method resulted in about one percent (30 r/min) speed drop at the point of full load injected which is smaller than about four percent (110 r/min) in classic method. It could be concluded that the proposed extended high-gain state

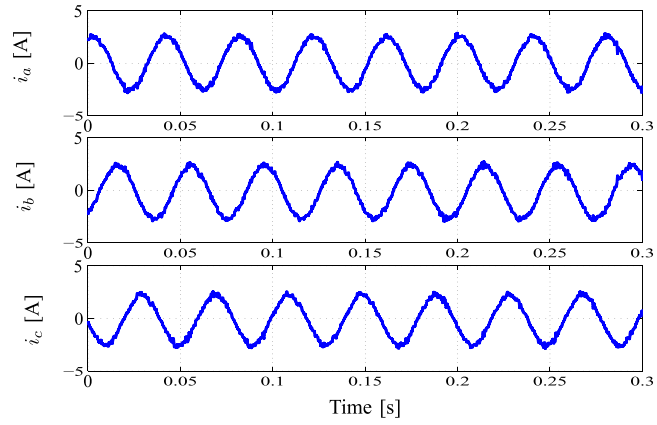

Fig. 11. Current waveforms of a, b, c phases under proposed method (THD $= 5.87\%$).

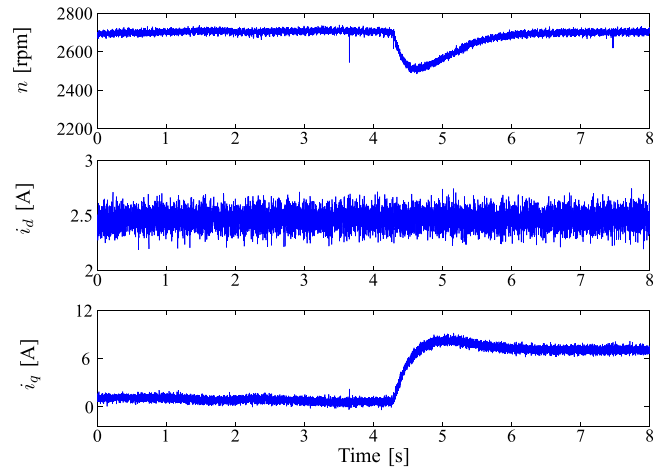

Fig. 12. Speed, i_d, and i_q waveforms at 2700 r/min with 7 Nm load disturbance under classic method.

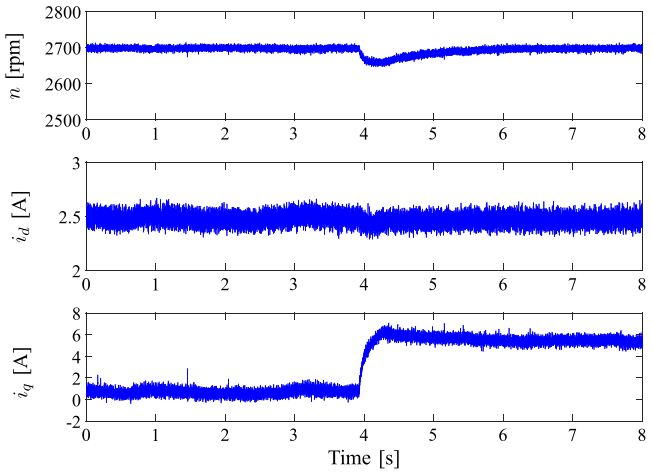

Fig. 13. Speed, i_d, and i_q waveforms at 2700 r/min with 7 Nm load disturbance under proposed method.

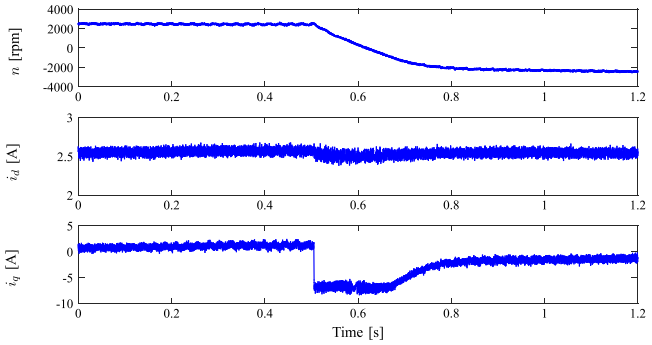

Fig. 14. Speed, i_d, and i_q waveforms at full speed reversal process.

observer works well for solving the problems of load disturbance and uncertainties. The ripples of i_d and i_q for the proposed one and the classical method are around 0.2 and 0.8 A, respectively. The ripples are partly generated by mechanical system when the motor rotates at high speeds. Lower current ripples verified that the new cost function helps the improvement of current qualities.

The second set of test is developed to observe the performance in the whole speed range for proposed method. The motor is operated to rotate from nominal speed to minus nominal speed. As a current controller, we observe speed, i_d and i_q in this operation. Fig. 14 shows the results. From the picture, we see that the proposed method works in a very big speed range. i_d has slight ripples that are less than 0.1 A. i_q has some oscillations, less than 1.0 A, which reflects the ripples of electromagnetic torque. This is normal when a motor rotates at a high speed. In the cost function, every phase current is controlled equally. Fig. 15 gives the result for a close look at the torque step process. The load changes from 2 to 7 Nm, the torque, i_q, i_d, and switching vectors are observed. The pictures show that the dynamic process is very fast. The settling time is less than 0.3 ms. The reason can be seen in the switching vectors shown in the picture. During the dynamic process, only non-zero vectors are selected, which is the direct reason for the implementation. However, the theory can be explained by the design of the proposed method. The inner controller uses a direct current control method, which ensures an unlimited bandwidth. Furthermore, the designed outer speed controller has no integral part. As discussed, the integral part is a slow process. Therefore, the proposed system is comparatively very fast. The following efforts will therefore be focused on the load impacts at different operation points in steady state. The test goes from low speed to full speed with load torque. At first, the motor rotates at 300 r/min. Then, a 7 Nm load is added to the system. Fig. 16 shows the resulting effects in the behaviors of speed, i_d, and i_q. It can be seen that the proposed method works well. The ripples on i_d and i_q are less than 0.1 and 0.5 A, respectively. According to our experience, on the same test benches, even DTC is difficult to work under this condition. The reason is easy to find as DTC assumes an adequately high speed reference. The proposed direct current control method has no problem in this case, either in theory or in the test results. Next, the motor rotates at 1500 r/min with a full load. Fig. 17 presents the effects on speed, i_d, and i_q. Compared with behaviors at 300 r/min, the ripples are slightly bigger as oscillation resulted from a middle speed range. However, i_d, and i_q ripples are still less than 0.1 and 0.6 A, respectively. It can therefore be concluded that the proposed system works in a very wide speed range with full loads, which is essential to drive systems.

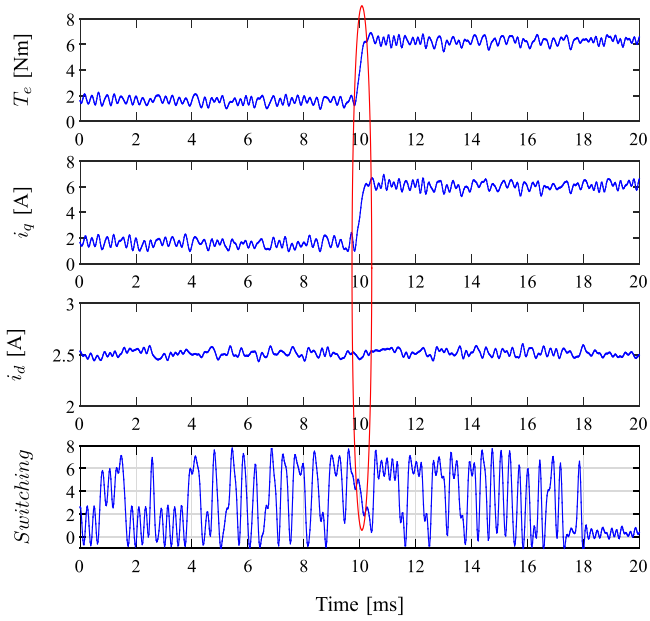

Fig. 15. Torque, i_q, i_d, and switching waveforms with a torque sudden altering.

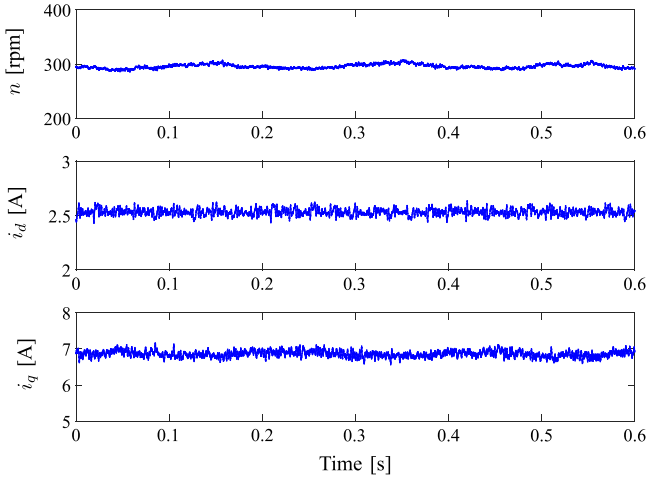

Fig. 16. Speed, i_d, and i_q waveforms at 300 r/min with 7 Nm load.

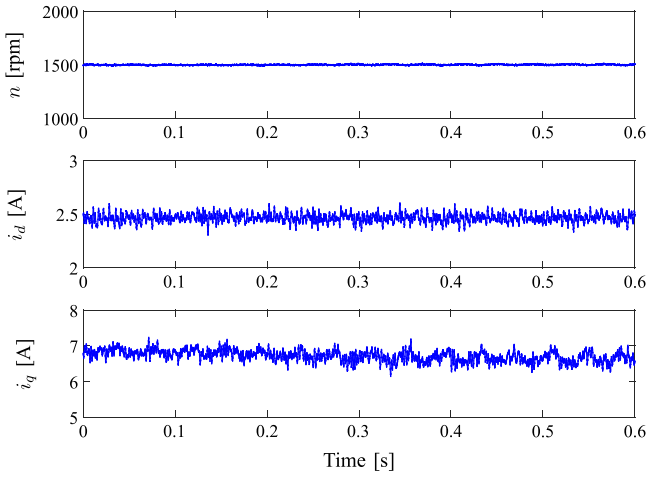

Fig. 17. Speed, i_d, and i_q waveforms at 1500 r/min with 7 Nm load.

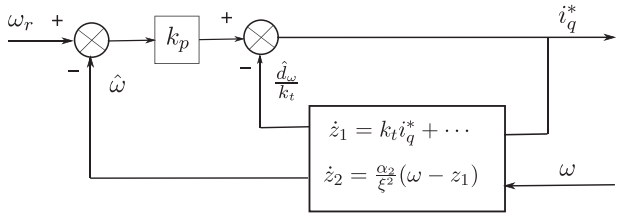

Fig. 18. Current reference of i_q^* is generated based on the EHGSO observer.

V. Conclusion

A disturbance estimation based direct current control method for the induction system has been proposed in this paper. The proposed method solves two problems. First, an inner current controller without weighting factors simplifies the system's tuning process. Second, this method eliminates the integral part, which is a slow process. An EHGSO observer method is designed as the speed controller of the IM system. From a theoretical standpoint, the performance of the proposed system is fast and stable. The tests verified that the proposed method works with the expected results in the whole speed range with both zero and full loads. The future work will investigate this direct current control strategy for the applications of multi-phase drive systems.

Appendix

After defining the cost function in (8), the next step is to calculate the reference values of $i_{a,b,c}$. As in FOC, we first calculate the current reference values in dq frame. The current reference i_d^* is set to be a constant value, which is calculated by $i_d^* = \frac{|\psi_r{}^*|}{L_m}$. An EHGSO observer based direct current control method for the induction system has been studied in this paper. By utilizing the disturbance estimation technique, an EHGSO-DCC controller has been developed. The load disturbance rejection ability is improved by the proposed design. The control system stability analysis of the EHGSO-DCC method is also given. The simulation and experimental results show that it not only makes the states of the closed-loop system obtain high qualities of steady state performance and dynamic response, but also provides expected load disturbance rejection ability against torque load disturbances without sacrificing nominal performance.

The current reference i_q^* for the speed controller is designed by the following:

$$i_q^* = Msat\left(\frac{k_p(\omega_r - \hat{\omega}) - \hat{d}_\omega/k_t}{M}\right) \tag{18}$$

which is generated by the disturbance estimation based feedforward controller, as shown in Fig. 18.

The current protection item $I_m(k+h)$ is defined as

$$I_m(k+h) = \begin{cases} 0, \text{if} |i(k+h)| \le |i_{\max}| \\ r \gg 0. \end{cases}$$

If the current absolute value of $|i(k+h)|$ is higher than its limited maximum value $|i_{\max}|$, no switching vector can be selected. That is to say, it can prohibit the induction motor system

from over-current operation. Thus, the constraint problem of the control system is addressed; this is also the advantage of the MPC method. In this paper, we consider only the one-step predictive FOC by using *N* equal to one. However, taking into account the algorithm of time-delay compensation, $(k+2)$ is used in the actual implementation.

The novel control scheme is described in Fig. 1; the cost function plays the key part in this predictive control algorithm. For the cost function of the predictive FOC method, the next-step stator flux $\hat{\psi}_s(k+1)$, rotor flux $\hat{\psi}_r(k+1)$, and the current must be calculated based on the system model. The aim of this section is to design the flux and current observers. Based on the feedback of stator current and voltage information, the stator flux and the rotor flux equations are rewritten as follows:

$$\frac{d}{dt}\psi_s = \upsilon_s - R_s \cdot i_s \tag{19}$$

$$\psi_r = \frac{L_r}{L_m}\left(\psi_s - \frac{L_s L_r - L_m^2}{L_r} i_s\right). \tag{20}$$

Combining (2)–(4), i_s and ψ_r, the rotor flux observer is designed as follows:

$$\frac{d}{dt}\hat{\psi}_r = \frac{L_m R_r}{L_r} \cdot i_s - \left(\frac{R_r}{L_r} - j \cdot \omega_e\right) \cdot \psi_r. \tag{21}$$

Based on the Euler discretization method, the discrete time rotor flux observer is rewritten as

$$\hat{\psi}_r(k+1) = \hat{\psi}_r(k) + T_s\left(-\left(\frac{R_r}{L_r} - j \cdot \omega_e\right) \cdot \psi_r(k) + \frac{L_m R_r i_s(k)}{L_r}\right). \tag{22}$$

The stator current observer is designed as follows:

$$\dot{\hat{i}}_s = -\frac{L_m^2 R_r}{(L_m^2 - L_r L_s)L_r} i_s + \frac{L_r}{L_m^2 - L_r L_s} R_s i_s - \frac{L_r}{L_m^2 - L_r L_s}\upsilon_s - \frac{L_m}{L_m^2 - L_r L_s}\left(\frac{R_r}{L_r - j\omega}\right)\psi_r \tag{23}$$

and the discrete time formation of the stator current observer is

$$\hat{i}_s(k+1) = \left(1 - \frac{T_s L_m^2 R_r}{(L_m^2 - L_r L_s)L_r}\right)\hat{i}_s(k) + \frac{T_s L_r R_s \hat{i}_s(k)}{L_m^2 - L_r L_s} - \frac{T_s L_r}{L_m^2 - L_r L_s}\upsilon_s(k) - \frac{T_s L_m}{L_m^2 - L_r L_s}\left(\frac{R_r \psi_r(k)}{L_r - j\omega}\right) \tag{24}$$

where T_s is the sampling period. In the real systems, considering the time-delay problem, $i(k+2)$ is used in the predictions so as to reduce the errors.

In the cost function, the current values in a, b, c frame are obtained by the inverse Clark and inverse Park transformations as follows:

$$\begin{pmatrix} a \\ b \\ c \end{pmatrix} = \sqrt{\frac{2}{3}} \begin{pmatrix} \cos(\theta) & -\sin(\theta) \\ -\frac{1}{2}\cos(\theta) + \frac{\sqrt{3}}{2}\sin(\theta) & \frac{1}{2}\sin(\theta) + \frac{\sqrt{3}}{2}\cos(\theta) \\ -\frac{1}{2}\cos(\theta) - \frac{\sqrt{3}}{2}\sin(\theta) & \frac{1}{2}\sin(\theta) - \frac{\sqrt{3}}{2}\cos(\theta) \end{pmatrix} \begin{pmatrix} d \\ q \end{pmatrix}$$

where θ is the rotating angle.

REFERENCES

[1] D. Casadei, F. Profumo, G. Serra, and A. Tani, "FOC and DTC: Two viable schemes for induction motors torque control," *IEEE Trans. Power Electron.*, vol. 17, no. 5, pp. 779–787, Sep. 2002.

[2] G. Pellegrino, E. Armando, and P. Guglielmi, "Direct flux field-oriented control of IPM drives with variable DC link in the field-weakening region," *IEEE Trans. Ind. Appl.*, vol. 45, no. 5, pp. 1619–1627, Aug. 2009.

[3] Y. Zhang, J. Zhu, Z. Zhao, W. Xu, and D. G. Dorrell, "An improved direct torque control for three-level inverter-fed induction motor sensorless drive," *IEEE Trans. Power Electron.*, vol. 27, no. 3, pp. 1502–1513, Mar. 2012.

[4] C. Xia, J. Zhao, Y. Yan, and T. Shi, "A novel direct torque control of matrix converter-fed PMSM drives using duty cycle control for torque ripple reduction," *IEEE Trans. Ind. Electron.*, vol. 61, no. 1, pp. 2700–2713, Jun. 2014.

[5] A. Abosh, Z. Zhu, and Y. Ren, "Reduction of torque and flux ripples in space-vector modulation based direct torque control of asymmetric permanent magnet synchronous machine," *IEEE Trans. Power Electron.*, vol. 32, no. 4, pp. 2976–2986, Apr. 2017.

[6] D. Mohan, X. Zhang, and G. Foo, "Three level inverter fed direct torque control of IPMSM with constant switching frequency and torque ripple reduction," *IEEE Trans. Ind. Electron.*, vol. 63, no. 12, pp. 7908–7918, Dec. 2016.

[7] J. Rodriguez, R. M. Kennel, J. R. Espinoza, M. Trincado, C. A. Silva, and C. A. Rojas, "High-Performance control strategies for electrical drives: An experimental assessment," *IEEE Trans. Ind. Electron.*, vol. 59, no. 2, pp. 812–820, Feb. 2012.

[8] P. Correa, M. Pacas, and J. Rodriguez, "Predictive torque control for inverter-fed induction machines," *IEEE Trans. Ind. Electron.*, vol. 54, no. 2, pp. 1073–1079, Apr. 2007.

[9] J. Rodriguez *et al.*, "Predictive current control of a voltage source inverter," *IEEE Trans. Ind. Electron.*, vol. 54, no. 1, pp. 495–503, Feb. 2007.

[10] M. Habibullah, D. Lu, D. Xiao, and M. F. Rahman, "A simplified finite-state predictive direct torque control for induction motor drive," *IEEE Trans. Ind. Electron.*, vol. 63, no. 6, pp. 3964–3975, Aug. 2016.

[11] M. Preindl and S. Bolognani, "Model predictive direct speed control with finite control set of PMSM drive systems," *IEEE Trans. Power Electron.*, vol. 28, no. 2, pp. 1007–1015, Feb. 2013.

[12] M. Preindl and S. Bolognani, "Model predictive direct torque control with finite control set for PMSM drive systems, Part 1: Maximum torque per ampere operation," *IEEE Trans. Ind. Inform.*, vol. 9, no. 4, pp. 1912–1921, Nov. 2013.

[13] R. Vargas, U. Ammann, B. Hudoffsky, and J. Rodriguez, "Predictive torque control of an induction machine fed by a matrix converter with reactive input power control," *IEEE Trans. Power Electron.*, vol. 25, no. 6, pp. 1426–1438, Jun. 2010.

[14] S. Davari, D. Khaburi, F. Wang, and R. M. Kennel, "Using full order and reduced order observers for robust sensorless predictive torque control of induction motors," *IEEE Trans. Power Electron.*, vol. 27, no. 7, pp. 3424–3433, Jul. 2012.

[15] T. Geyer, G. Papafotiou, and M. Morari, "Model predictive direct torque control—part I: Concept, algorithm, and analysis," *IEEE Trans. Ind. Electron.*, vol. 56, no. 6, pp. 1894–1905, Jun. 2009.

[16] T. Geyer, "Model predictive direct torque control: Derivation and analysis of the state-feedback control law," *IEEE Trans. Ind. Appl.*, vol. 49, no. 5, pp. 2146–2157, Sep. 2013.

[17] J. Scoltock, T. Geyer, and U. Madawala, "A comparison of model predictive control schemes for MV induction motor drives," *IEEE Trans. Ind. Inform.*, vol. 9, no. 2, pp. 909–919, May 2013.
[18] F. Wang, S. Li, X. Mei, W. Xie, J. Rodrguez, and R. M. Kennel, "Model based predictive direct control strategies for electrical drives: An experimental evaluation of PTC and PCC Methods," *IEEE Trans. Ind. Inform.*, vol. 11, no. 3, pp. 671–681, Jun. 2015.
[19] J. Holtz, "Advanced PWM and predictive control—An overview," *IEEE Trans. Ind. Electron.*, vol. 63, no. 6, pp. 3837–3844, Jun. 2016.
[20] J. Holz, "Sensorless control of induction machines with or without signal injections," *IEEE Trans. Ind. Electron.*, vol. 53, no. 1, pp. 7–30, Feb. 2006.
[21] Y. Zhang and H. Yang, "Two-Vector-Based model predictive torque control without weighting factors for induction motor drives," *IEEE Trans. Power Electron.*, vol. 31, no. 2, pp. 1381–1390, Feb. 2016.
[22] Y. Zhang, Y. Peng, and H. Yang, "Performance improvement of two-vector-based model predictive control of PWM rectifier," *IEEE Trans. Power Electron.*, vol. 31, no. 8, pp. 6016–6030, Aug. 2016.
[23] S. Kwak, U. Moon, and J. Park, "Predictive control based direct power control with an adaptive parameter identification technique for improved AFE performance," *IEEE Trans. Power Electron.*, vol. 29, no. 11, pp. 6178–6187, Nov. 2014.
[24] J. Rodriguez *et al.*, "Predictive current control of a voltage source inverter," *IEEE Trans. Ind. Electron.*, vol. 54, no. 1, pp. 495–503, Feb. 2007.
[25] H. Young, M. Perez, and J. Rodriguez, "Analysis of finite-control-set model predictive current control with model parameter mismatch in a three-phase inverter," *IEEE Trans. Ind. Electron.*, vol. 63, no. 5, pp. 3100–3107, May 2016.
[26] J. Rodriguez and P. Cortes, *Predictive Control of Power Converters and Electrical Drives*, 1st ed. Hoboken, NJ, USA: Wiley, 2012.
[27] Z. Xu and M. Rahman, "Comparison of a sliding observer and a Kalman filter for direct-torque-controlled IPM synchronous motor drives," *IEEE Trans. Ind. Electron.*, vol. 59, no. 11, pp. 4179–4188, Nov. 2012.
[28] A. Smith, S. Gadoue, and J. Finch, "Improved rotor flux estimation at low speeds for torque MRAS-based sensorless induction motor drives," *IEEE Trans. Energy Convers.*, vol. 31, no. 1, pp. 270–282, Nov. 2016.
[29] H. Yang, Y. Zhang, J. Liang, J. Liu, N. Zhang, and P. D. Walker, "Robust deadbeat predictive power control with a discrete-time disturbance observer for PWM rectifiers under unbalanced grid conditions," *IEEE Trans. Power Electron.*, vol. 34, no. 1, pp. 287–300, Jan. 2019.
[30] J. Han, "From PID to active disturbance rejection control," *IEEE Trans. Ind. Electron.*, vol. 56, no. 3, pp. 900–906, Mar. 2009.
[31] S. Li and Z. Liu, "Adaptive speed control for permanent-magnet synchronous motor system with variations of load inertia," *IEEE Trans. Ind. Electron.*, vol. 56, no. 8, pp. 3050–3059, Aug. 2009.
[32] H. Liu and S. Li, "Speed control for PMSM servo system using predictive functional control and extended state observer," *IEEE Trans. Ind. Electron.*, vol. 59, no. 2, pp. 1171–1183, Feb. 2012.
[33] W. Chen, "Disturbance observer based control for nonlinear systems," *IEEE/ASME Trans. Mechatronics*, vol. 9, no. 4, pp. 706–710, Dec. 2004.
[34] S. Li, J. Yang, W. Chen, and X. Chen, *Disturbance Observer-Based Control: Methods and Applications.* Boca Raton, FL, USA: CRC Press, 2014.
[35] B. Sun and Z. Gao, "A DSP-Based active disturbance rejection control design for a 1-kW H-bridge DC-DC power converter," *IEEE Trans. Ind. Electron.*, vol. 52, no. 5, pp. 1271–1277, Oct. 2005.
[36] M. Nakao, K. Ohnishi, and K. Miyachi, "Robust decentralized joint control based on interference estimation," in *Proc. IEEE Int. Conf. Robot. Automat.*, 1987, vol. 4, pp. 326–331.
[37] W. Chen, J. Yang, L. Guo, and S. Li, "Disturbance-Observer-Based control and related methods—An overview," *IEEE Trans. Ind. Electron.*, vol. 63, no. 2, pp. 1083–1095, Feb. 2016.
[38] H. Khail, *Nonlinear Systems*, 3rd ed. Upper Saddle River, NJ, USA: Prentice-Hall, 2002.

Fengxiang Wang (S'13–M'14–SM'18) was born in Jiujiang, China, in 1982. He received the B.S. degree in electronic engineering and the M.S. degree in automation from Nanchang Hangkong University, Nanchang, China, in 2005 and 2008, respectively, and the Ph.D. degree from the Institute for Electrical Drive Systems and Power Electronics, Technische Universitaet Muenchen, Munich, Germany, in 2014.

He is currently working with Haixi Institutes, Chinese Academy of Sciences, Jinjiang, China. His research interests include predictive control and sensorless control for electrical drives.

Junxiao Wang (S'14–M'18) was born in Wuxue, China, in 1986. He received the B.S. and M.S. degrees in control theory and control engineering from the Information Engineering College, Henan University of Science and Technology, Luoyang, China, in 2008 and 2011, respectively, and the Ph.D. degree in control theory and control engineering from the School of Automation, Southeast University, Nanjing, China, in 2017.

He was a Visiting Ph.D. Student with the Institute for Electrical Drive Systems and Power Electronics, Technical University of Munich, Munich, Germany, from September 2015 to September 2016. He is currently working with the College of Information Engineering, Zhejiang University of Technology, Hangzhou, China. His research interests include advanced control theory and its application to power electronics and motion control systems.

Dr. Wang was the recipient of 2017 IET Premium Award for Best Paper in IET Control Theory & Applications.

Ralph M. Kennel (M'89–SM'96) was born in Kaiserslautern, Germany, in 1955. He received the Diploma and the Dr.-Ing. (Ph.D.) degrees from the University of Kaiserslautern, Kaiserslautern, Germany, in 1979 and 1984, respectively.

From 1983 to 1999, he worked on several positions with Robert BOSCH GmbH, Stuttgart, Germany. Until 1997, he was responsible for the development of servo drives. He was one of the main supporters of VECON and SERCOS interface, two multi-company development projects for a microcontroller and a digital interface especially dedicated to servo drives. Furthermore, he took actively part in the definition and release of new standards with respect to CE marking for servo drives. Between 1997 and 1999, he was responsible for "Advanced and Product Development of Fractional Horsepower Motors" in automotive applications. His main activity was preparing the introduction of brushless drive concepts to the automotive market. From 1994 to 1999, he was appointed a Visiting Professor with the University of Newcastle-upon-Tyne, England, U.K. From 1999 to 2008, he was a Professor of electrical machines and drives with Wuppertal University, Wuppertal, Germany. Since 2008, he has been a Professor of electrical drive systems and power electronics with the Technical University of Munich, Munich, Germany. His main interests are: Sensorless control of ac drives, predictive control of power electronics, and hardware-in-the-loop systems.

Dr. Kennel is a Fellow of IET (IEE) and a Chartered Engineer in the U.K. Within IEEE, he was the Vice President of the Meetings of the Power Electronics Society (PELS) from 2007 to 2010. Since 2011, he is ECCE Global Chair of IEEE.-PELS, and since 2007 he is a Treasurer of the Germany Section.

José Rodríguez (M'81–SM'94–F'10) received the engineer degree in electrical engineering from the Universidad Tecnica Federico Santa Maria, Valparaiso, Chile, in 1977, and the Dr.-Ing. degree in electrical engineering from the University of Erlangen, Erlangen, Germany, in 1985.

He has been with the Department of Electronics Engineering, Universidad Tecnica Federico Santa Maria, since 1977, where he was a Full Professor and the President. Since 2015, he has been the President of the Universidad Andres Bello, Santiago, Chile. He has coauthored two books, several book chapters, and more than 400 journal and conference papers. His main research interests include multilevel inverters, new converter topologies, control of power converters, and adjustable-speed drives.

Dr. Rodríguez is a member of the Chilean Academy of Engineering. He was the recipient of a number of Best Paper Awards from journals of the IEEE. In 2014, he was the recipient of the National Award of Applied Sciences and Technology from the government of Chile. In 2015, he was the recipient of the Eugene Mittelmann Award from the Industrial Electronics Society of the IEEE.